The Astrophysical Journal Letters, 775:L38 (6pp), 2013 October 1 doi:10.1088/2041-8205/775/2/L38

NEAR-INFRARED ADAPTIVE OPTICS IMAGING OF INFRARED LUMINOUS GALAXIES: THE BRIGHTEST CLUSTER MAGNITUDE–STAR FORMATION RATE RELATION

Z. Randriamanakoto[1,2], A. Escala[3], P. Väisänen[1,4], E. Kankare[5], J. Kotilainen[5], S. Mattila[5], and S. Ryder[6]
[1] South African Astronomical Observatory, P.O. Box 9, 7935 Observatory, Cape Town, South Africa; zara@saao.ac.za
[2] Astronomy Department, University of Cape Town, Private Bag X3, Rondebosch 7701, South Africa
[3] Departamento de Astronomía, Universidad de Chile, Casilla 36-D, Santiago, Chile
[4] Southern African Large Telescope, P.O. Box 9, 7935 Observatory, Cape Town, South Africa
[5] Finnish Centre for Astronomy with ESO (FINCA), University of Turku, Väisäläntie 20, FI-21500 Piikkiö, Finland
[6] Australian Astronomical Observatory, P.O. Box 915, North Ryde, NSW 1670, Australia
Received 2013 August 12; accepted 2013 August 28; published 2013 September 12

ABSTRACT

We have established a relation between the brightest super star cluster (SSC) magnitude in a galaxy and the host star formation rate (SFR) for the first time in the near-infrared (NIR). The data come from a statistical sample of ∼40 luminous IR galaxies (LIRGs) and starbursts utilizing *K*-band adaptive optics imaging. While expanding the observed relation to longer wavelengths, less affected by extinction effects, it also pushes to higher SFRs. The relation we find, $M_K \sim -2.6 \log \mathrm{SFR}$, is similar to that derived previously in the optical and at lower SFRs. It does not, however, fit the optical relation with a single optical to NIR color conversion, suggesting systematic extinction and/or age effects. While the relation is broadly consistent with a size-of-sample explanation, we argue physical reasons for the relation are likely as well. In particular, the scatter in the relation is smaller than expected from pure random sampling strongly suggesting physical constraints. We also derive a quantifiable relation tying together cluster-internal effects and host SFR properties to possibly explain the observed brightest SSC magnitude versus SFR dependency.

Key words: galaxies: star clusters: general – galaxies: star formation – infrared: galaxies

1. INTRODUCTION

Young massive star clusters also known as super star clusters (SSCs) are a good tracer of the current star formation of the host galaxy (Portegies Zwart et al. 2010). Over the last decade, many studies have shown that there is an empirical relation between the *V*-band luminosity of the brightest cluster magnitude[7] and the global star-formation rate (SFR) of the galaxy (e.g., Larsen 2002; Weidner et al. 2004; Bastian 2008). Although various reasons have been suggested to explain the relation, they all highlight the important role star clusters play in understanding their host galaxy properties. Larsen (2002) and Whitmore (2003) emphasize the importance of size-of-sample effect in universal cluster formation, i.e., that large SSC populations preferentially sample the initial luminosity functions (LFs) to higher values, while Weidner et al. (2004) and Bastian (2008) show through theoretical simulations that effects from physical processes could also generate the observed correlation. Weidner et al. (2004) derive an expression which directly relates the total SFR of the galaxy with the mass of the brightest star cluster, with the assumption that the most massive cluster is always the brightest. On the other hand, Bastian (2008) argue that the youngest clusters are the brightest implying the tight observed relation is an imprint of the current SFR of the galaxy. Adamo et al. (2011) find that clusters in blue compact galaxies (BCGs) preferentially lie above the relation fit to more "normal" galaxies suggesting that the environments of SSCs play a role in determining the relation.

So far the validity of the relation has only been tested in the optical regime, and mostly using fairly nearby star-forming galaxies. Extinction effects are difficult to correct for especially in the dustier galaxies and will necessarily introduce scatter in the relation; using redder wavelengths will significantly improve the situation. With adaptive optics (AO) it is now possible to probe more distant host galaxies and thus increase the SFR baseline. Will the relation still hold in the near-infrared (NIR) and at larger SFR levels? Can we see effects of random sampling, and/or are there clear physical processes behind the relation? In this Letter, we use K_S-band (AO) imaging of 43 strongly star-forming galaxies to address these questions.

2. OBSERVATIONS AND PHOTOMETRY

Most of our sample, ∼30 galaxies, were imaged in the K_S-band with the NACO AO-instrument on the ESO Very Large Telescope (VLT).[8] The targets are *IRAS* galaxies from the RBGS (Sanders et al. 2003), selected to be $D_L \lesssim 200$ Mpc with IR luminosities above $\log (L_{\mathrm{IR}}/L_{\odot}) = 10.6$, and with a bright enough reference star near the field-of-view required by the AO system. The galaxies are hence a representative statistical sample of all IR-bright galaxies above $\log (L_{\mathrm{IR}}/L_{\odot}) = 10.6$ within the distance limit. They all have "cool" *IRAS* colors, though no active galactic nuclei were excluded a priori. Depending on the size of the galaxy, either the S27 or S54 camera was used, resulting in a pixel scale of 0.″027 pixel^{-1} or 0.″054 pixel^{-1}, respectively. The final point spread function (PSF) resolution was typically ∼0.″1. We used a dithering mode with 120 s per pointing, with total integration times per target ranging between 20 and 40 minutes.

Our `IRAF`-based pipeline was used to perform sky-subtraction. The individual frames were then aligned before average-combining them to get the final science image. We checked for image quality in individual frames and those with non-optimal AO-corrections were excluded, resulting in shorter total integration times in some cases (Table 1). Some frames with obviously non-photometric conditions were also excluded.

[7] Hereafter, we will refer to the "brightest cluster magnitude" as the "brightest cluster."

[8] Programs 086.B-0901 (PI: Escala) and 089.D-0847 (PI: Mattila).

Table 1
Observation log of the VLT/NACO and Gemini/NIRI *K*-band Data

Galaxy Name	Exp. Time (s)	D_L (Mpc)	$M_K^{\rm brightest}$ (mag)	log $L_{\rm IR}$ ($L_\odot$)	SFR ($M_\odot$ yr^{-1})
(1)	(2)	(3)	(4)	(5)	(6)
VLT/NACO data					
ESO 440−IG058-N	2280	102.0	−15.89	10.59†	6.6
IC 2522	1260	46.1	−15.52	10.63	7.3
MCG −02-01-052	1860	110.0	−17.21	10.63†	7.3
NGC 3620	1780	24.9	−15.65	10.70	8.5
ESO 428−G023	1770	44.5	−15.51	10.76	9.8
ESO 221−IG008	4620	46.7	−15.90	10.77	10.0
IRAS 06164 + 0311	1100	41.5	−16.06	10.79	10.5
NGC 1134	1240	47.4	−15.86	10.83	11.5
ESO 491−G020	1200	43.5	−17.47	10.86†	12.3
NGC 4433	1020	46.3	−16.39	10.87	12.6
NGC 1204	1100	61.4	−17.50	10.88	12.9
NGC 3508	1860	59.1	−16.42	10.90	13.5
NGC 1819	1950	61.9	−17.11	10.90	13.5
MCG −02-33-098	960	70.8	−15.69	10.95†	15.3
NGC 4575	720	45.0	−15.62	10.96	15.5
NGC 6000	2880	32.1	−16.36	10.97	15.8
ESO 550−IG025-S	1950	135.0	−16.76	11.03†	18.2
ESO 319−G020	960	43.2	−15.98	11.04	18.6
MCG +02-20-003	2340	70.5	−16.19	11.08	20.4
ESO 264−G057	1120	75.8	−17.15	11.08	20.4
ESO 320−G030	1120	49.0	−15.70	11.10	21.4
ESO 221−IG010	240	45.9	−17.19	11.17	25.1
ESO 267−G030	1920	80.9	−16.86	11.19	26.3
ESO 550−IG025-N	1950	135.0	−17.07	11.24†	29.5
ESO 440−IG058-S	2280	102.0	−17.79	11.28†	32.3
NGC 3110	2520	75.2	−17.74	11.31	34.7
IRAS 13052−5711	3480	91.6	−16.51	11.34	37.2
ESO 264−G036	2340	92.0	−17.98	11.35	38.1
IRAS 12116−5615	1800	117.0	−18.42	11.59	66.1
IRAS F06076−2139	1560	160.0	−19.61	11.59	66.1
IRAS 01173+1405	1320	127.0	−18.00	11.63	72.5
IRAS F01364−1042	1560	201.0	−20.01	11.76	97.8
IRAS 18293−3413	1230	74.6	−18.23	11.81	109.8
NGC 6240	720	103.0	−18.79	11.85	120.4
IRAS 19115−2124	1410	206.0	−19.71	11.87	126.0
Gemini/NIRI data					
IRAS F16516−0948	900	94.8	−18.10	11.24	29.5
CGCG 049−057	1680	56.4	−17.14	11.27	31.6
IRAS F17578−0400	1470	57.3	−17.56	11.35	38.1
MCG +08-11-002	1140	79.9	−17.52	11.41	43.7
IRAS F17138−1017	990	72.2	−18.48	11.42	44.7
NGC 3690	2192	45.3	−17.88	11.48†	51.6
IC 694	1260	45.3	−16.95	11.66†	77.4
IC 883	1440	101.0	−18.38	11.67	79.5

Notes. Column 1: IRAS survey name; Column 2: total exposure time; Column 3: luminosity distance from NED Database; Column 4: K_S-band absolute magnitude of the brightest cluster; Column 5: galaxy IR luminosity from Sanders et al. (2003), any value marked by † is estimated by using the method described in Section 3; Column 6: SFR derived from Equation (1).

Photometric zero-points were either retrieved from the ESO/NACO official Web site, if recorded, or estimated by correlating with Two Micron All Sky Survey K_S point-sources present in the field. Fields where both methods were available were used to check consistency of photometry. The zero-point uncertainty of ∼0.1 is included in resulting SSC photometry, which varies in the range ∼0.1–0.4 mag. The results are in a Vega-based system.

We added 12 other luminous IR galaxies (LIRGs) which form a homogeneous data set (same wavelength and similar depth and resolution) with the new sample described above. Eight of these come from Gemini-N/ALTAIR/NIRI and four from earlier NACO data.[9] The Gemini sample was selected with a higher $\log(L_{\rm IR}/L_\odot >)11.3$ cut-off; the final results are checked without these in case of any biases. Ten of these additional targets were published in Randriamanakoto et al. (2013) with the

[9] Programs 072.D-0433, 073.D-0406, 084.D-0261, 087.D-0444 for earlier NACO data; and GN-2008A-Q- 38, GN-2008B-Q-32, GN-2009A-Q-12, GN-2009B-Q-23, GN-2010A-Q-40 (PI: Ryder) for Gemini data.

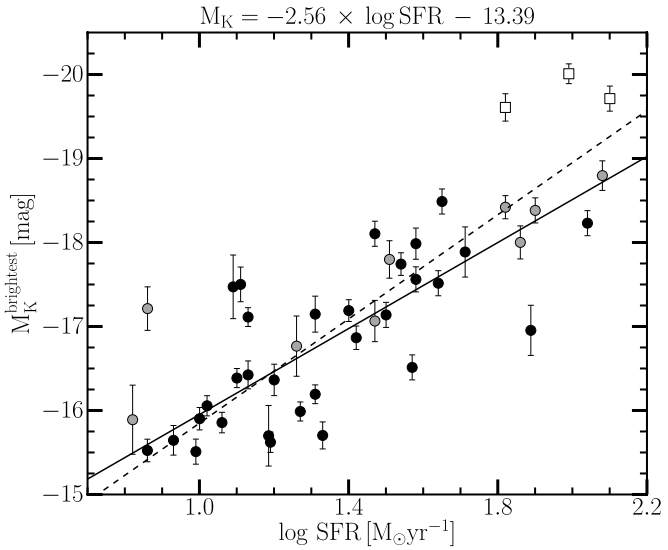

Figure 1. Empirical relation between the *K*-band magnitude of the brightest cluster and the SFR of the galaxy. The dashed line shows a weighted linear fit to all the data, including the three most distant targets at $D_L > 150$ Mpc shown as open squares. The solid line fits the $D_L \leqslant 150$ Mpc targets labeled as circles; those at $D_L \leqslant 100$ Mpc are black and those at $100 < D_L \leqslant 150$ Mpc are gray.

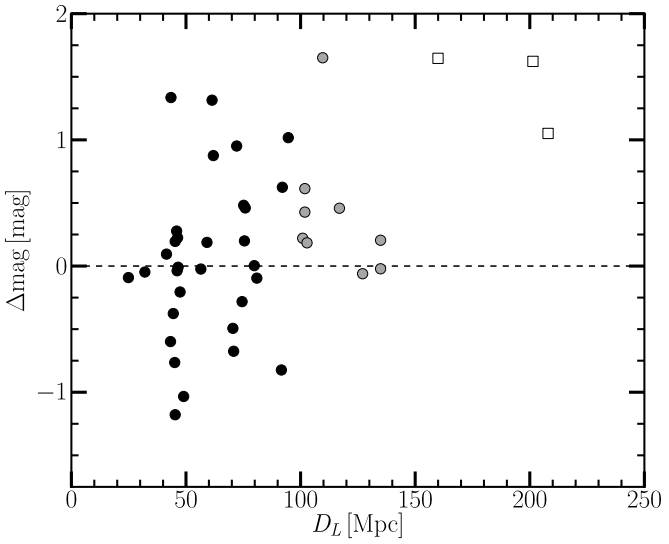

Figure 2. Dispersion about the fit in Figure 1, as a function of distance, from a relation such as shown in Figure 1 fit for targets closer than 80 Mpc. Symbols as in Figure 1.

SSC catalogs ready for analysis, and two unpublished targets are analyzed here (NGC 6240 and NGC 6000). We refer the reader to Mattila et al. (2007), Kankare et al. (2008, 2012), Väisänen et al. (2008a, 2008b), and Randriamanakoto et al. (2013) for details of observations and data reduction.

2.1. Photometry and SSC Selection

The SSC candidate photometric catalogs were generated by following the same steps as in Randriamanakoto et al. (2013). Briefly, an unsharp-masked version of the science image was used for object detection using `SExtractor` (Bertin & Arnouts 1996) with a configuration optimized to detect faint sources in very complex backgrounds. Photometry itself was then performed with `IRAF/PHOT` in aperture radii of 2 and 3 pixels (0.″11 and 0.″08) in frames taken with S54 and S27, respectively. The sky annuli were 1.5 and 2 pixels wide, respectively, with the inner radius one pixel away from the aperture radius in both cases. Aperture correction was achieved with the usual curve-of-growth method, drawn until ∼1″ radius. If there were enough isolated point sources in the field, this aperture correction was dependent on the distance to the AO reference star. Our SSC selection method retains only likely point-sources by utilizing the concentration of light in the detected sources. Simultaneously, we exclude likely foreground stars using visual inspection supported by expected star counts from the models of Besançon (Robin et al. 2003), as well as the nucleus, or nuclei, of the target galaxies.

3. RESULTS

Assuming, as usual, that the SFR of strongly star-forming galaxies is well represented by their IR luminosity, the following empirical relation by Kennicutt (1998) was used to convert the L_{IR} to SFR for each galaxy:

$$\frac{SFR}{M_\odot\ yr^{-1}} = 1.7 \times 10^{-10} L_{IR}\,(L_\odot). \quad (1)$$

Both values are listed in Table 1.

If the galaxy is a close pair or a multiple system, its IR luminosity has to be separated into individual components since the Sanders et al. (2003) values are for the whole system due to the poor spatial resolution of *IRAS*. Therefore, we used *WISE* 12 and 22 μm, *Spitzer*/MIPS 24 and 60 μm, and *Herschel*/PACS 70 μm archival data[10] to measure the flux from each galaxy component and the *IRAS*-based L_{IR} was redistributed according to the average ratio from all those wavelengths that were available and resolved. This method was adopted for these targets: ESO 440−IG058, MCG −02-01-052, MCG −02-33-098, ESO 491−IG020, ESO 550−IG025, IC 694/NGC 3690 (=Arp 299).

The NIR brightest cluster–SFR relation is shown in Figure 1. A weighted linear fit to *all* the points (the uncertainties of the resolved components' L_{IR} points were doubled) results in the following relation, shown as the dashed line in Figure 1:

$$M_K^{brightest} = -3.10 \times \log SFR - 12.75. \quad (2)$$

Blending effects may be a concern, however. The physical spatial resolution in our survey, corresponding to the ∼0.″1 PSF size, is typically 20–60 pc. Thus, individual detections of SSC candidates could potentially be blends of more than one intrinsic SSC. The effect may not be too severe for the brightest clusters, since Randriamanakoto et al. (2013) showed using Monte Carlo (MC) simulations that a single bright SSC will overwhelmingly dominate the luminosity of a SSC candidate detection when small apertures are used, except in the most distant targets approaching $D_L \sim 200$ Mpc, or in case of very strong clustering of SSC regions. Nevertheless, we check for blending effects in the following way: the M_K versus SFR relation was fit for the "safe" galaxies at $D_L \leqslant 80$ Mpc (the slope is −2.50 in this case), and Figure 2 then plots the *difference* of the brightest M_K from this best-fit relation versus the distance of the host. If distance plays no part, a scatter plot is expected. Indeed, no systematics are seen, apart from the three most distant targets falling significantly above the null-hypotheses line. We interpret this as the brightest SSC in those three targets potentially being

[10] http://irsa.ipac.caltech.edu, http://herschel.esac.esa.int

contaminated by other clusters and exclude them from further analysis. We obtain a new best fit (solid line in Figure 1) when using a $D_L \leqslant 150$ Mpc constraint:

$$M_K^{\rm brightest} = -2.56 \times \log {\rm SFR} - 13.39. \quad (3)$$

The slope varies in the range -2.49 to -2.56 with distance limits set in between 80 and 150 Mpc. The formal uncertainty of the slope is ± 0.07 and the scatter of the observed M_K values is $\sigma \approx 0.62$ mag. The slope *without* the eight Gemini galaxies is -2.43; the difference is within $\sim 1.5\sigma$ of the overall fit and does not affect any conclusions.

4. DISCUSSION

4.1. Statistical Interpretation

It has been suggested that the $M^{\rm brightest}$–SFR relation in the V-band can be explained in purely statistical terms (Larsen 2002). To explore this possibility in the NIR, $M_K^{\rm brightest}$ is plotted against the number of SSC candidates brighter than a certain absolute magnitude level. We select $M_K = -15$ mag since at that level we do not yet need completeness corrections. The result can be seen in Figure 3. This correlation is consistent with the idea that the more clusters are forming in a galaxy, the higher will be the probability to sample the brightest ones from a given LF of the overall population (Larsen 2002). The empirical relation can also be tied to the slope of the LF. If the $L^{\rm max}$ of the most luminous object scales with the total number N of the clusters as given by Whitmore (2003)

$$L^{\rm max} \sim N^{\eta}, \quad (4)$$

then by using the equation from Hunter et al. (2003)

$$\eta = \frac{1}{\alpha - 1}, \quad (5)$$

we can derive the power-law slope α of the cluster LF at higher luminosities. The best-fit $\eta = 0.64$ corresponds to $\alpha = 2.56$ which is not unreasonable for bright parts of SSC LFs (Portegies Zwart et al. 2010). From the 10 LIRGs in Randriamanakoto et al. (2013) we found a slope of $\alpha \sim 1.9$ (flatter than for normal spirals) which corresponds to $\eta = 1.1$—this is overplotted in Figure 3 as the dashed line and is seen to represent the data at $\log N > 0.5$ fairly well.

The scatter of $\sigma \sim 0.62$ mag in Figure 1 is smaller than in relations derived in the optical showing $\sigma \sim 1$ mag (Larsen 2002), unsurprising since extinction effects are smaller. Given that the SFR determination uncertainties should be of the order of 0.4 dex, the observed scatter is surprisingly small, however. We ran MC simulations where a given LF with no physical upper limit was sampled purely randomly and the magnitude of the brightest cluster was recorded. The $M^{\rm brightest}$ distribution is narrower with steeper LFs parameterized with the power-law index α. In particular, we find $\sigma = 1.15$ for $\alpha = 2.0$, and $\sigma = 0.77$ and 0.58 for $\alpha = 2.5$ and 3.0, respectively, each with uncertainties of ≈ 0.02. In case of purely statistical sampling the scatter in our relation must hence be the result of steeper than observed LFs of $\alpha > 2.5$—or there are other physical characteristics at play which determine the luminosity of the brightest cluster.

In summary, while the characteristics of the number of detected SSCs versus SFR are consistent with a size-of-sample effect, the tightness of the brightest cluster versus SFR relation in particular suggests that it would be premature to reject an underlying physical cause for this relation.

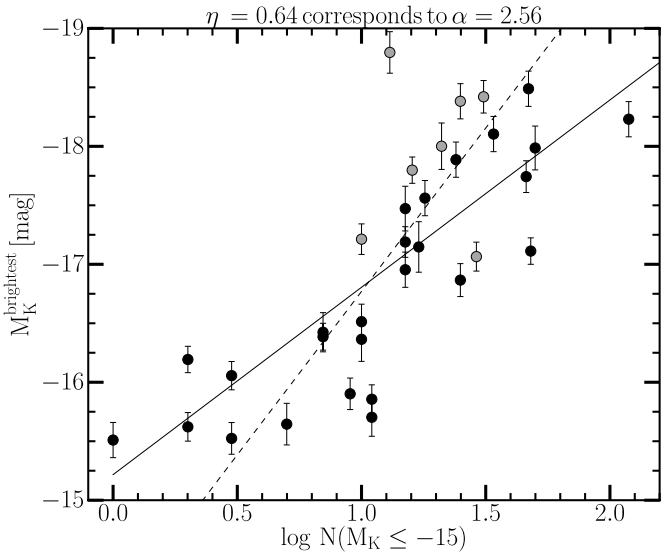

Figure 3. $M_K^{\rm brightest}$ as a function of the number of SSCs brighter than -15 mag for targets with $D_L \leqslant 150$ Mpc. The solid line is the best-fit relation, whereas the dashed line corresponds to a LF power-law slope of $\alpha = 1.9$. Symbols as in Figure 1.

4.2. Physical Interpretation

Clusters are born of collapsing giant molecular clouds which inevitably are affected by their galactic environments, especially in cases of interacting and merging galaxies—how this environment exactly defines SSC properties, and disruption, is a matter of intense debate (e.g., Lamers 2009). Specifically regarding the brightest cluster versus SFR relation, Adamo et al. (2011) have shown how SSCs in BCGs appear elevated from the general relation, and suggest this could be a result of a higher cluster formation efficiency in their extreme environments. Larsen (2009) and Gieles (2009) suggest that the characteristic cluster mass may change as a function of environment, and grow in the more intense SFR of interactions and mergers. One appealing possibility for such a change is the lack of large scale rotation in galaxy mergers (Escala & Larson 2008; Weidner et al. 2010; Escala et al. 2013).

In addition, there might well be internal constraints on SSC properties. In the following we outline a possible physical interpretation of the brightness versus SFR relation based on the idea that the total luminosity, and mass, of a stellar cluster is weighted toward its highest mass stars, and these stellar masses may also be correlated with the environments of the clusters (e.g., Weidner et al. 2009).

The total luminosity of a cluster can be computed for a given initial mass function (IMF) and mass–luminosity relation. Assuming a mass–luminosity relation of the form $L \propto {\rm m}^{\alpha_{\rm l}}$ and a power-law IMF ($dN/dm \propto m^{-\beta}$), the total luminosity of a cluster is given by

$$L_{\rm tot} \propto M_{\rm cl}^{(\alpha_{\rm l}-\beta+1)\gamma}, \quad (6)$$

where $M_{\rm cl}$ is the total mass of the cluster, which is assumed to satisfy a relation with the most massive star of such cluster: $M_{\rm star}^{\rm max} \sim M_{\rm cl}^{\gamma}$, being $\gamma \sim 0.45$ estimated from observations and $\gamma \sim 2/3$ predicted from simulations (see Weidner et al. 2009 for a review on different estimates).

Assuming that the most massive unstable gas cloud in a galaxy, $M_{\rm cloud}^{\rm max} \sim f_{\rm gas}^2 M_{\rm gas}$ (Escala & Larson 2008), leads to

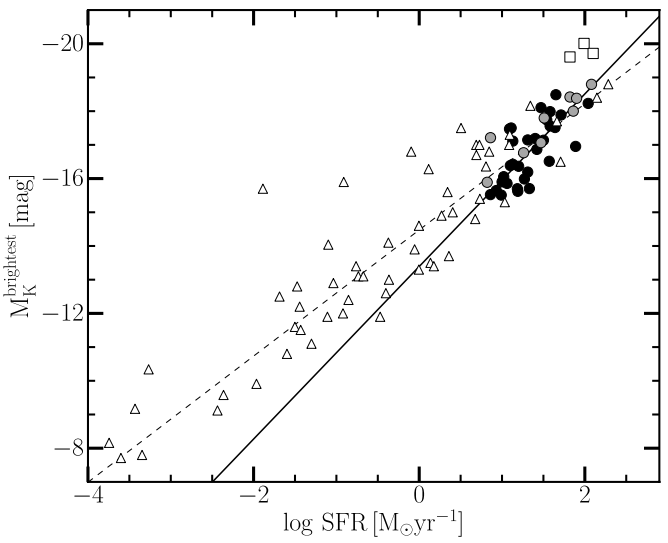

Figure 4. $M^{brightest}$–SFR relation with data from literature (the triangles; Adamo et al. 2011 and references therein) added to the present work (symbols as in Figure 1). The solid line is our best fit of Equation (3) and the dashed line is the fit from Weidner et al. (2004) to the optical V-band data after a constant $V-K=2$ conversion.

the formation of the most massive SSC ($M_{cl} \propto M_{cloud}^{max}$) and taking into account the correlation between such a cloud and the SFR in galaxies, SFR $\propto [M_{cloud}^{max}]^{\delta}$ with $\delta \sim 1.5$ (Escala 2009, 2011), the total luminosity of the brightest cluster is given by $L_{tot}^{brightest} \propto SFR^{(\alpha_1-\beta+1)\gamma/\delta}$. Finally, this can be expressed in terms of absolute magnitude by $M_K^{brightest} \propto -2.5 \log L_K^{brightest}$, resulting in:

$$M_K^{brightest} \propto -2.5 \frac{(\alpha_1 - \beta + 1)\gamma}{\delta} \log SFR. \quad (7)$$

For a Salpeter IMF ($\beta = 2.35$), $\delta = 1.5$ (Escala 2009, 2011), $\gamma \sim 0.45$ estimated from observations (Weidner et al. 2009) and a slope of the mass–luminosity relation of $\alpha_1 \sim 5$, Equation (7) gives a slope closer to -3 in the brightest cluster–SFR relation, which is comparable to the slope observed if we use the whole sample (Equation (2)). On the other hand, for a slope of the mass–luminosity relation of $\alpha_1 \sim 4$, Equation (7) gives a slope ~ -2, which is closer to that derived from our data excluding potentially blended cases (Equation (3)).

Unfortunately, we do not have a good estimate for the slope of the mass–luminosity relation α_1 at high masses—it may, for example, vary in between 1.76 and 8.87 depending on the highest mass of a star in a cluster for masses larger than 7 $M_\odot$ (Parravano et al. 2003). Nevertheless, Equation (7) may be used as a simple physical interpretation of the effects characterizing SSC properties at scales ranging from internal to galactic.

4.3. Comparison to the V-band Relation

Figure 4 shows the brightest cluster–SFR relation with an expanded scale. The triangles are V-band data as compiled by Adamo et al. (2011), assuming a constant $V-K=2$ conversion, typical for a ∼10 Myr age stellar population. The solid line is the best-fit slope of -2.56 from our own NIR data extrapolated to lower SFRs. It appears that the optical points would require a slightly flatter slope, and indeed Weidner et al. (2004) find ~ -1.9 shown as the dashed line, though Larsen (2002) derives ~ -2.5 from a subset of the data. The simplest explanation could perhaps be extinction: the highest SFR galaxies, LIRGs and ultraluminous IR galaxies, are predominantly interactions and mergers with more dust on average than lower SFR galaxies (Piqueras López et al. 2013). The uncorrected optical points at higher SFR could lie too low artificially, thus flattening the slope. However, with this data set alone it is not possible to confirm this—it could as well be that the brightest clusters detected in V-band are not necessarily (always) the most luminous clusters in K-band possibly implying age effects. That the *slope* appears slightly different necessarily points to some systematic effects along the SFR base-line, i.e., a constant $V-K$ shift is not appropriate.

The slope may become steeper if the points at higher SFR, preferentially, are bound results of mergers of individual SSCs in very dense star cluster complexes (Fellhauer & Kroupa 2005). We also note that outliers *below* the relation can be understood as cases where the brightest SSC is not detected, or is severely extincted. As discussed by Bastian (2008), outliers *above* the line may be cases where the detected cluster is significantly *older* than the general population of brightest SSCs. These are very interesting questions to tackle with combinations of optical and NIR data in the future.

5. SUMMARY AND FUTURE WORK

From a K-band AO sample of 43 strongly star-forming galaxies, mostly LIRGs, we establish the brightest cluster magnitude–SFR relation in the NIR regime. The relation is much less affected by extinction effects than similar comparisons in the V-band. We find a slope of -2.56 which is similar to those from optical derivations made at lower SFR levels, though the extension of our slope appears to not be consistent with the full range of optical SSC luminosities if a single $V-K$ conversion is adopted. We suggest that a systematic extinction effect, where SSCs in higher SFR hosts live in dustier environments, would be a simple explanation for the trend, but systematic age differences may also be involved.

A good correlation of the most luminous cluster and the number of SSCs with M_K magnitude brighter than -15 shows that a size-of-sample effect is broadly consistent with the observed $M_K^{brightest}$–SFR relation. On the other hand, the observed scatter in the relation is surprisingly small, and we show that it can be explained with random sampling effects *only* if the LF of SSCs is very steep at the bright end, steeper than usually observed. Hence, physical reasons determining the luminosity of the brightest SSC from host properties, and/or internal cluster effects, likely play a role as well. We derived a relation tying the stellar IMF and mass–luminosity relations together with the global SF properties of the host in explaining the observed brightest cluster magnitude–SFR relation.

In the next steps of the work, we will investigate in more detail the environments and extinctions of the host galaxies, and masses and ages of the SSCs inside them, with a combination of optical and NIR data and kinematic information. These will allow more secure disentanglement of the various physical effects governing the lives and characteristics of SSCs in galaxies.

We thank the anonymous referee for the valuable comments and suggestions to improve this work. Z.R. acknowledges funding from the South African Square Kilometre Array, A.E. from the Financiamiento Basal Grant PFB 06, FONDECYT Grant 1130458 and Anillo de Ciencia y Tecnologia Grant

ACT1101, and P.V. from the National Research Foundation. Based on observations made with the ESO Telescopes at the La Silla Paranal Observatory, Chile. Based in part on observations obtained at the Gemini Observatory, which is operated by the Association of Universities for Research in Astronomy, Inc., under a cooperative agreement with the NSF on behalf of the Gemini partnership: the National Science Foundation (United States), the National Research Council (Canada), CONICYT (Chile), the Australian Research Council (Australia), Ministério da Ciência, Tecnologia e Inovação (Brazil), and the Ministerio de Ciencia, Tecnología e Innovación Productiva (Argentina).

REFERENCES

Adamo, A., Östlin, G., & Zackrisson, E. 2011, MNRAS, 417, 1904
Bastian, N. 2008, MNRAS, 390, 759
Bertin, E., & Arnouts, S. 1996, A&AS, 117, 393
Escala, A. 2009, arXiv:0909.4318
Escala, A. 2011, ApJ, 735, 56
Escala, A., Becerra, F., del Valle, L., & Castillo, E. 2013, ApJ, 763, 39
Escala, A., & Larson, R. B. 2008, ApJL, 685, L31
Fellhauer, M., & Kroupa, P. 2005, ApJ, 630, 879
Gieles, M. 2009, MNRAS, 394, 2113
Hunter, D. A., Elmegreen, B. G., Dupuy, T. J., & Mortonson, M. 2003, AJ, 126, 1836
Kankare, E., Mattila, S., Ryder, S., et al. 2008, ApJL, 689, L97
Kankare, E., Mattila, S., Ryder, S., et al. 2012, ApJL, 744, L19
Kennicutt, R. C., Jr. 1998, ARA&A, 36, 189
Lamers, H. J. G. L. M. 2009, Ap&SS, 324, 183
Larsen, S. S. 2002, AJ, 124, 1393
Larsen, S. S. 2009, A&A, 494, 539
Mattila, S., Väisänen, P., Farrah, D., et al. 2007, ApJL, 659, L9
Parravano, A., Hollenbach, D. J., & McKee, C. F. 2003, ApJ, 584, 797
Piqueras López, J., Colina, L., Arribas, S., & Alonso-Herrero, A. 2013, A&A, 553A, 85
Portegies Zwart, S. F., McMillan, S. L. W., & Gieles, M. 2010, ARA&A, 48, 431
Randriamanakoto, Z., Väisänen, P., Ryder, S., et al. 2013, MNRAS, 431, 554
Robin, A. C., Reylé, C., Derrière, S., & Picaud, S. 2003, A&A, 409, 523
Sanders, D. B., Mazzarella, J. M., Kim, D., Surace, J. A., & Soifer, B. T. 2003, AJ, 126, 1607
Väisänen, P., Mattila, S., Kniazev, A., & Adamo, A. 2008a, MNRAS, 384, 886
Väisänen, P., Ryder, S., Mattila, S., & Kotilainen, J. 2008b, ApJL, 689, L37
Weidner, C., Bonnell, I. A., & Zinnecker, H. 2010, ApJ, 724, 1503
Weidner, C., Kroupa, P., & Larsen, S. S. 2004, MNRAS, 350, 1503
Weidner, C., Kroupa, P., & Maschberger, T. 2009, MNRAS, 393, 663
Whitmore, B. C. 2003, in A Decade of Hubble Space Telescope Science, ed. M. Livio, K. Noll, & M. Stiavelli (Cambridge: Cambridge Univ. Press), 153